Electronic Supplementary Material (ESI) for Journal of Materials Chemistry A.

Supporting Information for:

Carbon-supported metal nanodendrites as efficient, stable catalysts for the oxygen reduction reaction

Luna B. Venarusso[1], Chirley V. Boone[1], Jefferson Bettini[2], Gilberto Maia[1]*

[1]Institute of Chemistry, Universidade Federal de Mato Grosso do Sul; Av. Senador Filinto Muller, 1555; Campo Grande, MS 79074-460, Brazil.

[2]Brazilian Nanotechnology National Laboratory (LNNano); Rua Giuseppe Máximo Scolfaro, 10000; Campinas, SP 13083-100, Brazil.

*To whom correspondence should be addressed.

Table S1. Initial and EDX metal masses, TG metal masses (unburned), and TG and EDX mass percentages of MND/C nanocomposites.

	Initial mass (mg)	Initial mass (%)	EDX metal mass (%)	TG metal mass, unburned (%)	TG and EDX masses (%)
Pt/C	C: 16 Pt: 4	C: 80 Pt: 20	Pt: 100	19.2	C: 80.8 Pt: 19.2
Pt'/C	C: 16 Pt: 4 Ni: 0.8	C: 76.9 Pt: 19.2 Ni: 3.9	Pt: 100	18.7	C: 81.3 Pt: 18.7
Pt–Pd/C	C: 16 Pt: 4 Pd: 1.4	C: 74.8 Pt: 18.7 Pd: 6.5	Pt: 68.4 Pd: 31.6	25.8	C: 74.1 Pt: 17.7 Pd: 8.2
Pt@Au/C	C: 16 Pt: 4 Au: 2.6	C: 70.8 Pt: 17.7 Au: 11.5	Pt: 62.1 Au: 37.9	32.9	C: 67.1 Pt: 20.4 Au: 12.5
Pt–Pd'/C	C: 16 Pt: 4 Pd: 1.4 Ni: 0.8	C: 72.1 Pt: 18.0 Pd: 6.3 Ni: 3.6	Pt: 68.6 Pd: 31.4	26.6	C: 73.4 Pt: 18.2 Pd: 8.4
Pt–Pd@Au/C	C: 16 Pt: 4 Pd: 1.4 Au: 2.6	C: 66.7 Pt: 16.7 Pd: 5.8 Au: 10.8	Pt: 47.8 Pd: 21.6 Au: 30.6	34.7	C: 65.3 Pt: 16.6 Pd: 7.5 Au: 10.6
Pt@Au'/C	C: 16 Pt: 4 Au: 2.6 Ni: 0.8	C: 68.4 Pt: 17.1 Au: 11.1 Ni: 3.4	Pt: 57.9 Au: 42.1	29.4	C: 70.6 Pt: 17.0 Au: 12.4
Pt–Pd@Au'/C	C: 16 Pt: 4 Pd: 1.4 Au: 2.6 Ni: 0.8	C: 64.5 Pt: 16.1 Pd: 5.7 Au: 10.5 Ni: 3.2	Pt: 46.2 Pd: 25.5 Au: 28.3	31.0	C: 69.0 Pt: 14.3 Pd: 7.9 Au: 8.8

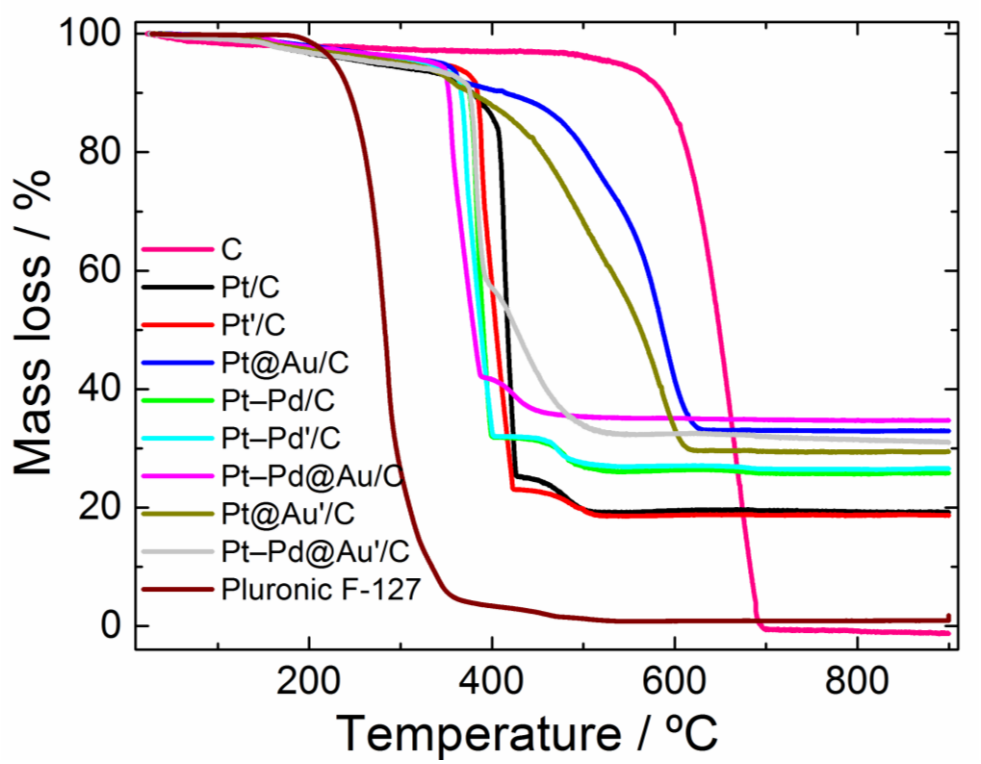

Fig. S1. TG responses for Vulcan Carbon XC-72 (C), Pluronic F-127, and MND/C (burning).

S1. Electrochemical profile

Figure S2 shows cyclic voltammograms for bare CG and GC electrodes modified with Vulcan Carbon XC-72, Pt(10 wt.%) on carbon, and E-Tek Pt/C (20% Pt mass), recorded in N_2-saturated 0.1 M $HClO_4$. For bare GC, no faradaic responses were detected within the 0.05-1.2 V potential region. When the GC electrode is modified with Vulcan Carbon XC-72 or Pt(10 wt.%) on carbon, the region of electrical double layer, formed at an electrolyte–electrode interface, behaves approximately as an ideal electrical capacitor [1, 2], storing charge when voltage is applied and, therefore, exhibiting higher capacitive currents. Pt electrochemical features were virtually absent from GC modified with Pt(10 wt.%) on carbon (Figure S3). For the GC electrode modified with E-Tek Pt/C (20% Pt mass), however, CV behavior is very similar to that observed for GC modified with MND/Cs (Figure 5).

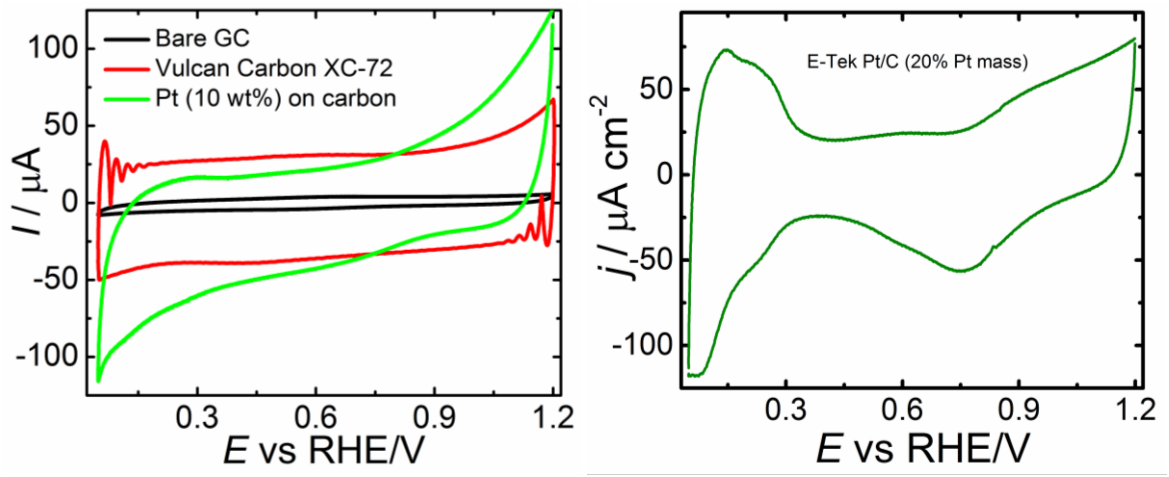

Fig. S2. Cyclic voltammograms for bare CG and GC electrodes modified with Vulcan Carbon XC-72, Pt(10 wt.%) on carbon, and E-Tek Pt/C (20% Pt mass), recorded in N_2-saturated 0.1 M $HClO_4$. Scan rate: 50 mV s^{-1}. Scans started at 1.2 V.

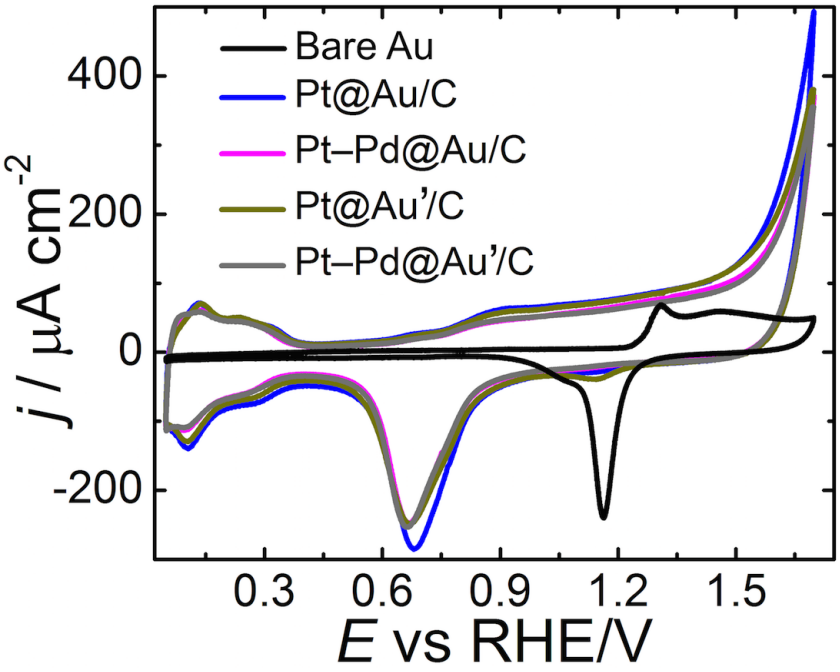

Fig. S3. Cyclic voltammograms for bare Au and GC electrodes modified with MND/Cs, recorded in N_2-saturated 0.1 M $HClO_4$. Scan rate: 50 mV s^{-1}. Scans started at 0.05 V. The graph depicts final CVs, recorded after all electrochemical experiments were performed. CVs are normalized to the electrochemically active surface area (*ECSA*).

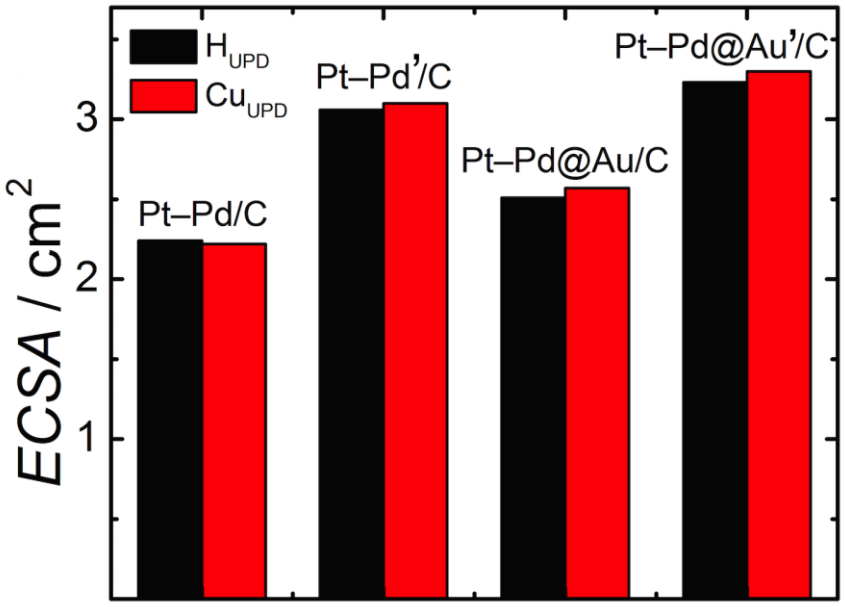

Fig. S4. Comparison of *ECSA* values calculated from H_{UPD}- and Cu_{UPD}-stripping for GC electrodes modified with Pt−Pd/C, Pt−Pd'/C, Pt−Pd@Au/C, and Pt−Pd@Au'/C nanocomposites.

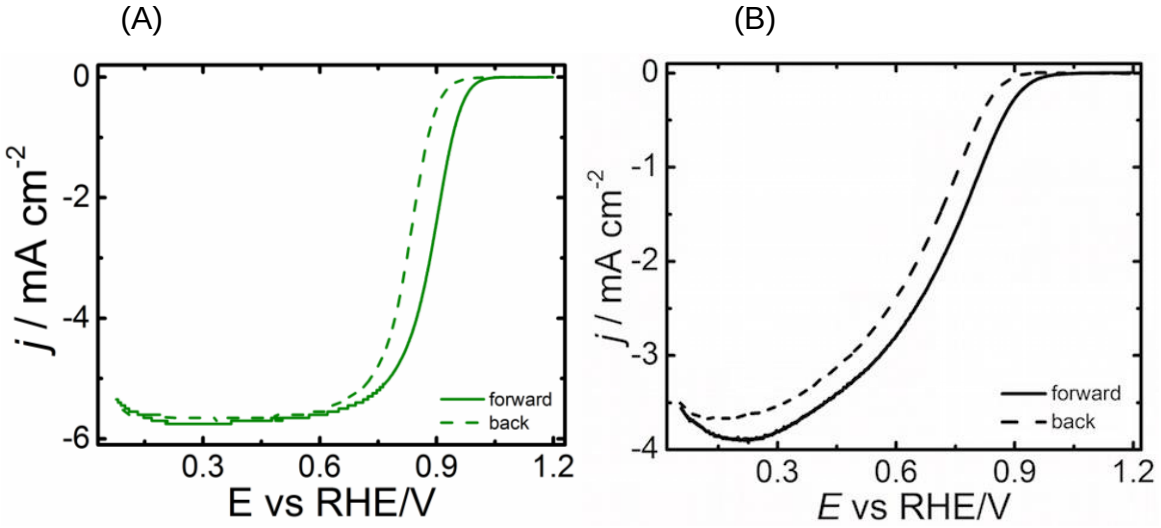

Fig. S5. Hydrodynamic cyclic voltammogram for (A) a modified E-Tek Pt/C (20% Pt mass)/GC electrode and (B) a Pt(10 wt.%)-on-carbon/GC electrode in O_2-saturated 0.1 M $HClO_4$ at ν = 10 mV s^{-1} and 1600 rpm.

Specific activity (*SA*, in mA cm^{-2}) [3, 4] was calculated as follows:

$$SA = \frac{\frac{I\ x\ I_d}{I_d - I}}{ECSA} = \frac{I_K}{ECSA} \quad \text{(S1)}$$

where I is the measured current and I_d and I_k are the diffusion-limited and kinetic currents, respectively.

MSA (mA μg^{-1}) was determined from the I_k value divided by A_g (the geometric GC surface area, cm^2) and by L_{PGM} (the Pt-group metal loading of the working electrode, mg cm^{-2}) [3, 4]:

$$MSA = \frac{I_k}{L_{PGM} A_g} \quad \text{(S2)}$$

Specific *ECSA* calculation was based on the following relation [3-6]:

$$Specific\ ECSA = \frac{ECSA}{L_{PGM}\ A_g} \quad \text{(S3)}$$

Table S2. $E_{1/2}$, PGM loading (L_{PGM}), *MSA*, specific *ECSA*, *SA*, and *ECSA* values from the present study and retrieved literature.

	$E_{1/2}$ (V)	L_{PGM} (μg_{PGM} cm^{-2})	*MSA* at 0.90 $V_{iR\text{-}free}$ ($mA\ \mu g^{-1}$)	Specific *ECSA* ($m^2\ g^{-1}$)	*SA* at 0.90 $V_{iR\text{-}free}$ ($mA\ cm^{-2}$)	*ECSA* (cm^2)	Ref.
Pt/C	**0.92**	29	0.53	46	1.16	2.6	Present study
Pt/C after 10 000 cycles	**0.92**	29	0.53	45	1.19	2.6	Present study
Pt'/C	**0.92**	28	0.43	45	0.94	2.5	Present study
Pt–Pd/C	**0.92**	39	0.34	29	1.17	2.2	Present study
Pt@Au/C	**0.92**	31	0.33	36	0.91	2.2	Present study
Pt–Pd'/C	**0.91**	41	0.29	38	0.76	3.1	Present study
Pt–Pd@Au/C	**0.91**	37	0.21	35	0.61	2.5	Present study
Pt@Au'/C	**0.93**	26	0.56	65	0.86	3.3	Present study
Pt@Au'/C after 10 000 cycles	**0.92**	26	0.53	39	1.35	2.0	Present study
Pt–Pd@Au'/C	**0.92**	34	0.33	48	0.69	3.2	Present study
Pt–Pd@Au'/C after 10 000 cycles	**0.91**	34	0.32	39	0.82	2.6	Present study
E-Tek Pt/C (20% Pt mass)	**0.89**	31	0.13	46	0.29	2.8	Present study
Octahedral PtNiCo/C	**-**	7.65	2.33	61.6	3.88	-	7
Carbon-supported PtNiCo alloy nanohexapod catalyst (PNCH/C)	**-**	10	0.8	-	1.6	-	8
Dendritic PtCuNi cubes (PtCuNi/C)	**0.921**	10	0.63 at 0.92 V	63.8	0.97 at 0.92 V	-	9
Pd_1Pt_5 dendrites (Pd_1Pt_5/C)	**0.88**	16 of Pt	0.192	61.06	0.314	-	10
Pt-based icosahedral nanocages	**-**	11.2 of Pt	1.28	36.5	3.5	-	11
$Pd@Pt_{2.7L}$/C	**-**	30.6	0.64	47.1	1.36	-	12
Pd@Pt−Ni/C with octahedral core−shell nanocrystals	**-**	12.3 of Pt	0.48	178.01	0.45	4.29	13

PdPt/C alloy, Pd@Pt/C core–shell	**0.884**	62.11	0.216	46.7	0.215	-	14
Pd_3Au@Pt/C	**-**	10.1	0.25	-	-	-	15
Rhombic dodecahedral AuPt@Pt bimetallic nanocrystals with dendritic branches	-	30	0.24	43	0.55	-	16
Pt-Pd-Cu/GNRs (graphene nanoribbons)	**0.95**	46	0.70 at 0.93 V	54	1.3 at 0.93 V	4.9	17
Porous nanostars of Pt–Pd@Au'	**0.95**	88.4	0.46	37	1.24	6.5	18
Pt@Au nanocrystals	**0.93**	50.4	0.41	34	1.22	3.3	19

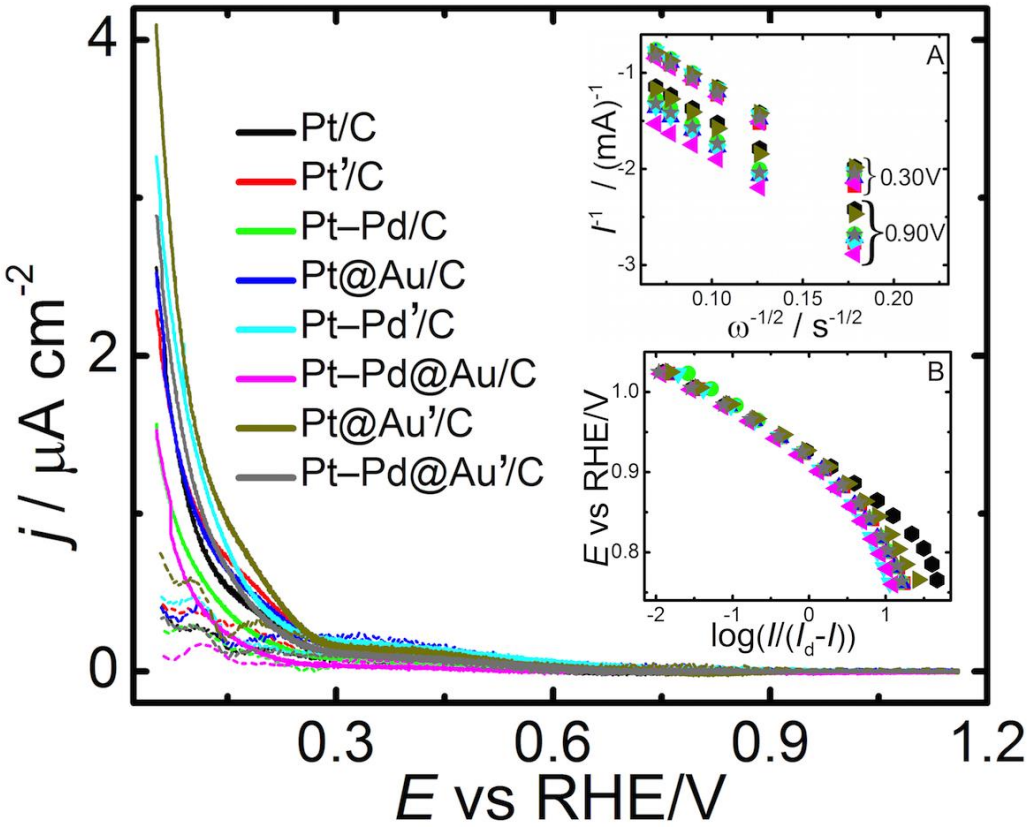

Fig. S6. Current density responses calculated per geometric area for a bare Au ring electrode maintained at 1.2 V, coupled with disk HCV for GC electrodes modified with MND/C nanocomposites in O_2-saturated 0.1 M $HClO_4$. ω = 1600 rpm; scan rate: 10 mV s^{-1}. Scans started at 0.05 V. Inset: (A) Koutecký–Levich plots obtained from forward hydrodynamic linear potential scan curves for GC electrodes modified with MND/C nanocomposites, in O_2-saturated 0.1 M $HClO_4$ (same curves as in Figure S8). (B) Tafel plots obtained from data in Figure S8 (ω = 1600 rpm).

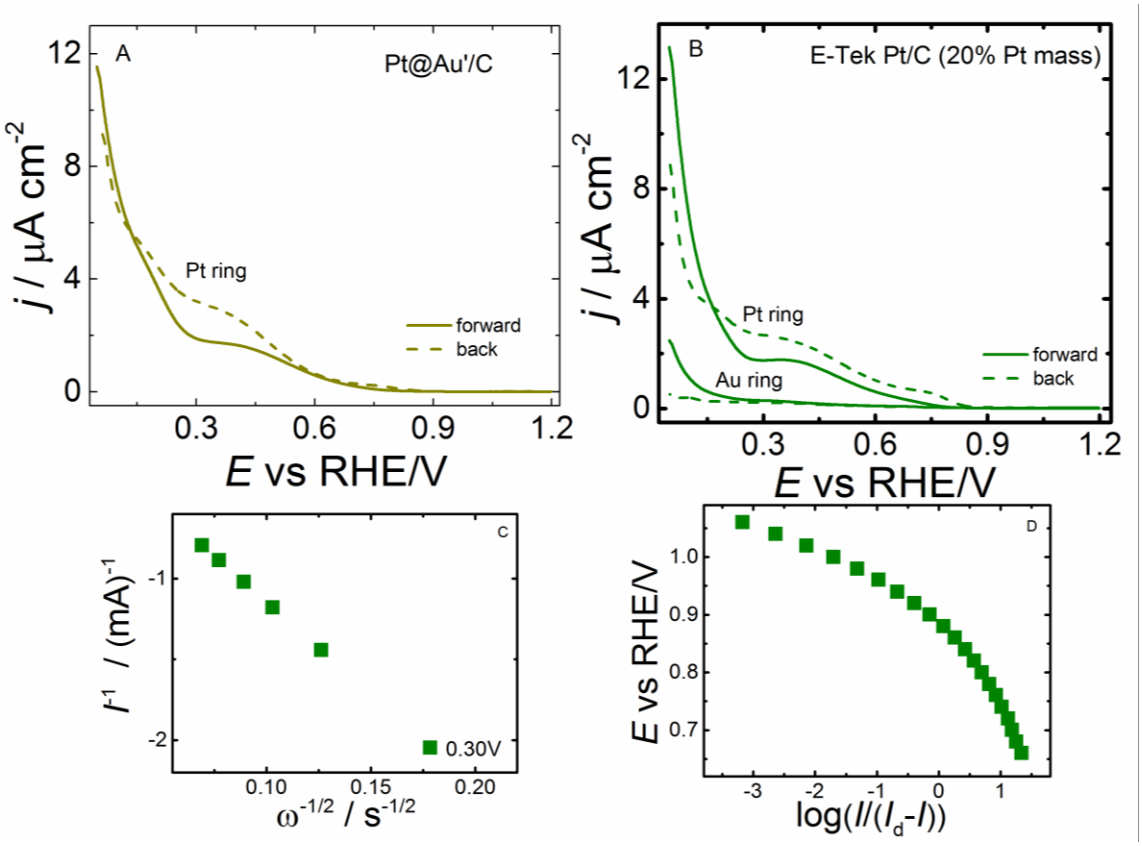

Fig. S7. Current density responses calculated per geometric area for a bare Pt (or Au) ring electrode maintained at 1.2 V, coupled with disk HCV for GC electrodes modified with (A) Pt@Au'C and (B) E-Tek Pt/C (20% Pt mass) in O_2-saturated 0.1 M $HClO_4$. ω = 1600 rpm; scan rate: 10 mV s^{-1}. Scans started at 0.05 V. (C) Koutecký–Levich plot obtained from forward hydrodynamic linear potential scan curves for a GC electrode modified with E-Tek Pt/C (20% Pt mass), in O_2-saturated 0.1 M $HClO_4$ (data not shown). (B) Tafel plots obtained from data in Figure S5A.

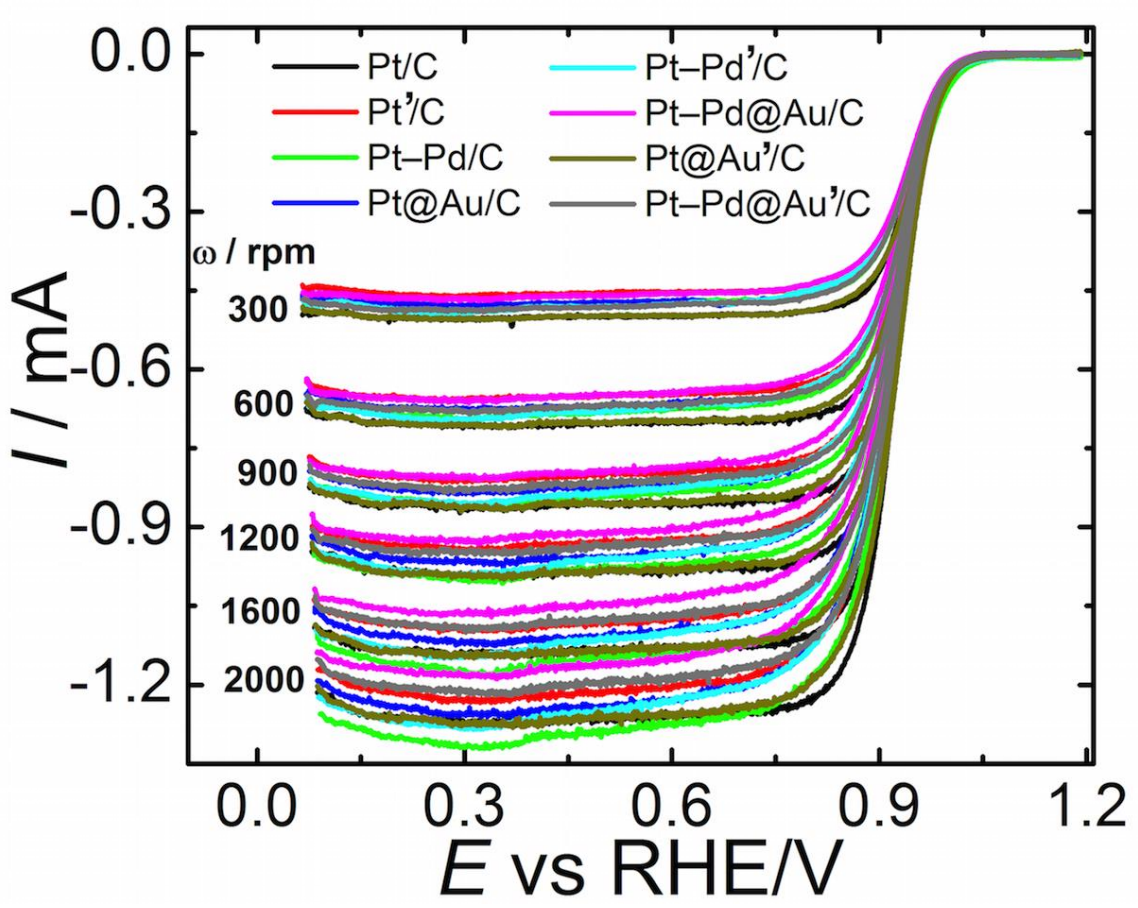

Fig. S8. Hydrodynamic voltammograms for modified GC electrodes in O_2-saturated 0.1 M $HClO_4$. Scan rate: 10 mV s^{-1}. Scans started at 0.05 V.

The percentage of H_2O_2 formation, $X_{H_2O_2}$, can be calculated from the molar flux rates of O_2, $\dot{n}_{O_{2(4e-)}}$, and H_2O_2, $\dot{n}_{O_{2(2e-)}}$, according to Eqs. S3 and S4 [3, 20]:

$$\dot{n}_{O_{2(4e-)}} = \frac{I_{H_2O}}{4F} \quad \text{and} \quad \dot{n}_{O_{2(2e-)}} = \frac{I_{H_2O_2}}{2F} \tag{S4}$$

$$X_{H_2O_2} = \frac{\dot{n}_{O_2\,(2e-)}}{\dot{n}_{O_2\,(2e-)} + \dot{n}_{O_2\,(4e-)}} = \frac{\frac{2\,I_R}{N}}{I_D + \frac{I_R}{N}} \tag{S5}$$

where $I_{H_2O} = I_D - I_{H_2O_2}$, $I_{H_2O_2} = I_R N^{-1}$, and $N = -\frac{I_R}{I_D}$, such that I_{H_2O} and $I_{H_2O_2}$ are the currents for O_2 reduction to water and H_2O_2, respectively; F is the Faraday constant (96 485 C mol^{-1}); I_R and I_D are the ring and disk currents, respectively; and N is the collection efficiency (0.26). H_2O_2 synthesis declined to negligible levels above 0.30 V (Figure S6).

Koutecký–Levich plots (Figure S6B) were obtained using Eq. S6 [21]:

$$\frac{1}{I} = \frac{1}{I_k} + \frac{1}{I_d} = \frac{1}{nF(ECSA)k\,C_{O_2}^b} - \frac{1}{0.62nFAD_{O_2}^{\frac{2}{3}}\nu^{-\frac{1}{6}}C_{O_2}^b\omega^{\frac{1}{2}}} \quad \text{(S6)}$$

where *n* is the number of electrons transferred per O_2 molecule, *ECSA* is the electrochemically active surface area, *A* is the electrode geometric area, *k* is the rate constant for O_2 reduction, $C_{O_2}^b$ is the oxygen concentration in the solution (1.2×10^{-6} mol cm^{-3})[22, 23], D_{O_2} is the oxygen diffusion coefficient in the medium (1.9×10^{-5} cm^2 s^{-1}) [22, 23], ν is the kinematic viscosity of the solution (0.01 cm^2 s^{-1}) [24], and ω is the rotation rate.

Table S3. Values of *n* for modified GC electrodes, calculated from ORR, based on slopes of Koutecký–Levich plots (Figure S6A) obtained at 0.30 V and 0.90 V on the second term on the right-hand side of Equation S6, and Tafel slopes (Figure S6B) from ORR for GC electrodes modified with MND/C electrocatalysts.

			Tafel slopes*	
GC electrodes modified with MND/C electrocatalysts	*n* (0.30 V)	*n* (0.90 V)	Low *I* (mV dec^{-1})	High *I* (mV dec^{-1})
Pt/C	4.0	4.0	–60	–116
Pt'/C	4.0	4.0	–61	–123
Pt–Pd/C	4.0	4.0	–64	–125
Pt@Au/C	4.0	4.0	–61	–122
Pt–Pd'/C	4.0	4.0	–59	–124
Pt–Pd@Au/C	4.0	4.0	–62	–120
Pt@Au'/C	4.0	4.0	–61	–118
Pt–Pd@Au'/C	4.0	4.0	–59	–124
E-Tek Pt/C (20% Pt mass)	4.0	–	–62	–121

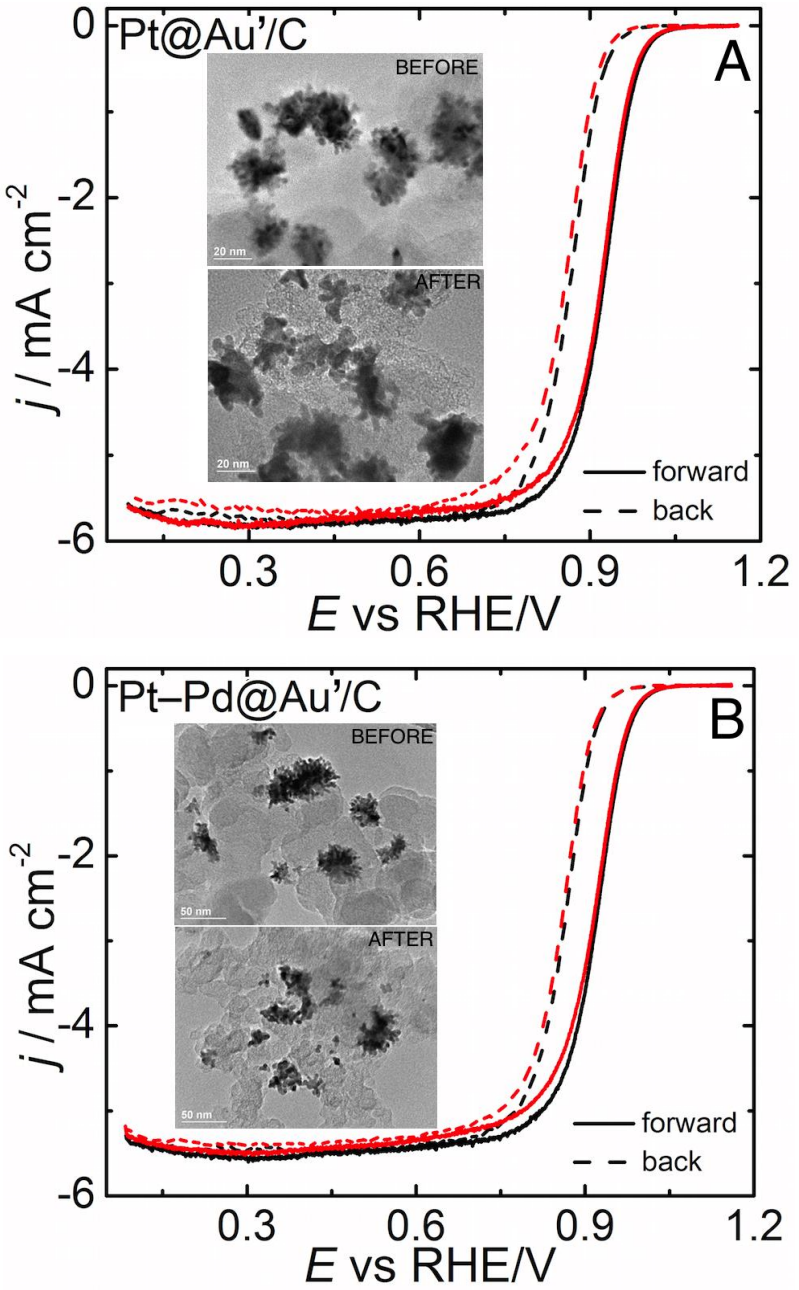

Fig. S9. Hydrodynamic cyclic voltammograms for GC electrodes modified with (A) Pt@Au'/C and (B) Pt–Pd@Au'/C electrocatalysts before and after the stability test (10 000 cycles between 0.6 and 1.0 V at 50 mV s^{-1}), in O_2-saturated 0.1 M $HClO_4$. ω = 1600 rpm; scan rate: 10 mV s^{-1}. Scans started at 0.05 V. Inset: Representative TEM images for Pt@Au'/C and Pt–Pd@Au'/C electrocatalysts before and after 10 000 potential scans.

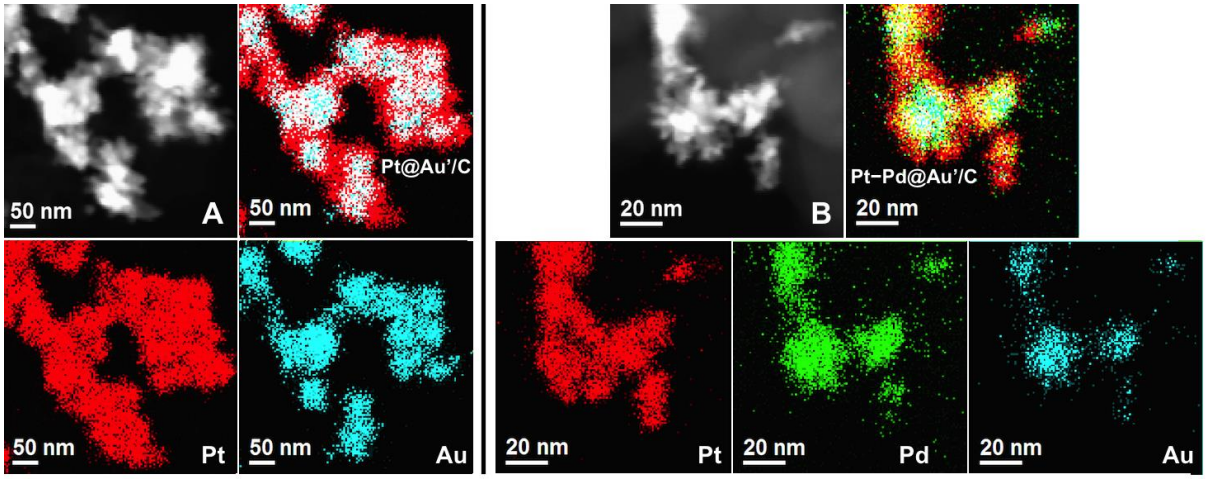

Fig. S10. Representative EDX mapping images for MND/Cs after 10 000 potential scans. (A) Pt@Au'/C; (B) Pt−Pd@Au'/C.

References

[1] B. E. Conway, *Electrochemical Supercapacitors - Scientific Fundamentals and Technological Applications*, Kluwer Academic / Plenum Publisher, New York, 1999.
[2] J. R. Miller, R. A. Outlaw and B. C. Holloway, *Science*, 2010, **329**, 1637.
[3] L. B. Venarusso, R. H. Sato, P. A. Fiorito and G. Maia, *J. Phys. Chem. C*, 2013, **117**, 7540.
[4] G. V. Fortunato, L. B. Venarusso and G. Maia, *ChemElectroChem*, 2014, **1**, 625.
[5] Y. Garsany, O. A. Baturina, K. E. Swider-Lyons and S. S. Kocha, *Anal. Chem.*, 2010, **82**, 6321.
[6] B. Lim, M. Jiang, P. H. C. Camargo, E. C. Cho, J. Tao, X. Lu, Y. Zhu and Y. Xia, *Science*, 2009, **324**, 1302.
[7] X. Huang, Z. Zhao, Y. Chen, E. Zhu, M. Li, X. Duan and Y. Huang, *Energy Environ. Sci.*, 2014, **7**, 2957.
[8] A. Oh, Y. Jin Sa, H. Hwang, H. Baik, J. Kim, B. Kim, S. H. Joo and K. Lee, *Nanoscale*, 2016, **8**, 16379.
[9] Y. Kuang, Y. Zhang, Z. Cai, G. Feng, Y. Jiang, C. Jin, J. Luo and X, Sun, *Chem. Sci.*, 2015, **6,** 7122.
[10] Y. Ye, J. Joo, S. Lee and J. Lee, *J. Mater. Chem. A*, 2014, **2**, 19239.
[11] X. Wang, L. F.-Cosme, X. Yang, M. Luo, J. Liu, Z. Xie and Y. Xia, *Nano Lett.*, 2016, **16**, 1467.
[12] X. Wang, S.-I. Choi, L. T. Roling, M. Luo, C. Ma, L. Zhang, M. Chi, J. Liu, Z. Xie, J. A. Herron, M. Mavrikakis and Y. Xia, *Nat. Commun.*, 2015, **6**:**7594**, DOI: 10.1038/ncomms8594.
[13] X. Zhao, S. Chen, Z. Fang, J. Ding, W. Sang, Y. Wang, J. Zhao, Z. Peng and J. Zeng, *J. Am. Chem. Soc.,* 2015, **137**, 2804.
[14] Y. Lim, S. K. Kim, S.-C. Lee, J. Choi, K. S. Nahm, S. J. Yoo and P. Kim, *Nanoscale*, 2014, **6**, 4038.
[15] H. Li, R. Yao, D. Wang, J. He, M. Li and Y. Song, *J. Phys. Chem. C*, 2015, **119**, 4052.
[16] L. Zhang, S. Yu, J. Zhang and J. Gong, *Chem. Sci.*, 2016, **7**, 3500.
[17] C. V. Boone and G. Maia, *Electrochim. Acta*, 2017, **247**, 19.
[18] L. B. Venarusso, J. Bettini and G. Maia, *ChemElectroChem*, 2016, **3**, 749.

[19] L. B. Venarusso, J. Bettini and G. Maia, *J. Solid State Electrochem*., 2016, **20**, 1753.
[20] U. A. Paulus, T. J. Schmidt, H. A. Gasteiger and R. J. Behm, *J. Electroanal. Chem*., 2001, **495**, 134–145.
[21] A. J. Bard, L. R. Faulkner in Electrochemical Methods: Fundamentals and Applications, John Wiley & Sons, New York, 2001.
[22] R. E. Davis, G. L. Horvath and C. W. Tobias, *Electrochim. Acta*, 1967, **12**, 287–297.
[23] R. R. Adžić, J. Wang and B. M. Ocko, *Electrochim. Acta*, 1995, **40**, 83–89.
[24] D. R. Lide in CRC Handbook of Chemistry and Physics, 82nd ed., CRC Press, Boca Raton, 2001.